Neuron, Vol. 31, 903–912, September 27, 2001, Copyright ©2001 by Cell Press

A Miniature Head-Mounted Two-Photon Microscope: High-Resolution Brain Imaging in Freely Moving Animals

Fritjof Helmchen,[1,4] Michale S. Fee,[1] David W. Tank,[1,5] and Winfried Denk[1,2,3]
[1] Biological Computation Research Department
Bell Laboratories
Lucent Technologies
Murray Hill, New Jersey 07974
[2] Department of Biomedical Optics
Max-Planck-Institute for Medical Research
69120 Heidelberg
Germany

Summary

Two-photon microscopy has enabled anatomical and functional fluorescence imaging in the intact brain of rats. Here, we extend two-photon imaging from anesthetized, head-stabilized to awake, freely moving animals by using a miniaturized head-mounted microscope. Excitation light is conducted to the microscope in a single-mode optical fiber, and images are scanned using vibrations of the fiber tip. Microscope performance was first characterized in the neocortex of anesthetized rats. We readily obtained images of vasculature filled with fluorescently labeled blood and of layer 2/3 pyramidal neurons filled with a calcium indicator. Capillary blood flow and dendritic calcium transients were measured with high time resolution using line scans. In awake, freely moving rats, stable imaging was possible except during sudden head movements.

Introduction

Various optical microscopy techniques have been used to visualize electrical and biochemical computation in neurons and their dendritic processes (Yuste et al., 1999). Dendritic excitability, for example, has been studied using fluorescence imaging of calcium-sensitive indicators (Regehr and Tank, 1994; Denk et al., 1996; Eilers and Konnerth, 1997). These experiments significantly contributed to our current understanding of dendrites as active, nonlinear elements which integrate synaptic inputs in a complex manner (Yuste and Tank, 1996; Häusser et al., 2000). Most of this imaging work has, however, been carried out in acute or cultured brain slice preparations, which, while preserving the local cellular context, disrupt long-range connections. Recently, dendritic activity of neocortical neurons has been measured in vivo in anesthetized animals, using fixed two-photon microscopes (Svoboda et al., 1997, 1999; Helmchen et al., 1999). Yet, even there, with all circuits structurally intact, anesthesia alters cortical dynamics and, in turn, single-cell activity, which depends on synaptic background activity, inhibition (Pare et al., 1998), and neuromodulation. Our knowledge about the behavior of cortical neurons in awake animals almost exclusively stems from action potential firing patterns measured with extracellular electrodes. Such recordings are, however, largely blind to the dendritic events involved in synaptic integration (but see Buzsaki and Kandel, 1998). A method for fluorescence imaging with subcellular resolution in the brain of awake, behaving animals would therefore be of great utility for studying the cellular computations underlying cortical function.

Two major obstacles make it difficult to apply optical microscopy to awake animals. First, and applicable to both the anesthetized and awake brain, is strong scattering of light by neural tissue. This problem is reduced in two-photon microscopy because of excitation with near-infrared light. In addition, two-photon excitation is confined to the focal plane, permitting efficient fluorescence detection (Denk et al., 1995). Due to these properties, two-photon microscopy has been the method of choice for obtaining optical sections relatively deep in neural tissue; imaging depths of $\sim$0.5 mm have been achieved in neocortex (Svoboda et al., 1997; Kleinfeld et al., 1998). As a second problem, there are brain pulsations and movements, which cause motion artifacts and prevent stable imaging. This problem is manageable in anesthetized animals but is exacerbated in awake animals (Fee, 2000). Movement artifacts are expected to be especially severe in freely moving animals, with the question arising whether in unrestrained animals stable imaging on the cellular scale is possible at all. Imaging of dendritic activity has been possible in awake, behaving insects, which are, however, easily immobilized due to their exoskeleton (Borst and Egelhaaf, 1992; Sobel and Tank, 1994; Single and Borst, 1998). Furthermore, taking advantage of the transparency of the larval zebrafish, calcium transients were measured in the immobilized zebrafish during escape behavior (O'Malley et al., 1996). Although imaging in awake, head-restrained mammals is conceivable with a fixed two-photon microscope, such experiments would inevitably suffer from a rather limited behavioral repertoire. The alternative route, which we have chosen, is to develop a microscopy technique that enables high-resolution imaging in freely behaving animals.

In freely moving animals, miniaturization of the imaging device so that the animal can carry it around is obviously an absolute prerequisite. For example, miniature CCD cameras have been attached to the skull or implanted in the brain. In those experiments, changes in light reflectance and scattering could be detected but not at cellular resolution (Rector et al., 1993, 1997). Various light-weight confocal microscopes have been built using fiber optic beam delivery (Delaney and Harris, 1995; Sabharwal et al., 1999), but none of them has been applied to in vivo imaging of neurons. Here, we present a miniaturized two-photon microscope that is based on fluorescence excitation through an optical fiber and a novel fiber-scanning mechanism. We describe the design of the two-photon fiberscope and demonstrate its

[3] Correspondence: denk@mpimf-heidelberg.mpg.de
[4] Present address: Department of Cell Physiology, Max-Planck-Institute for Medical Research, 69120 Heidelberg, Germany.
[5] Present address: Department of Molecular Biology and Department of Physics, Princeton University, Princeton, New Jersey 08540.

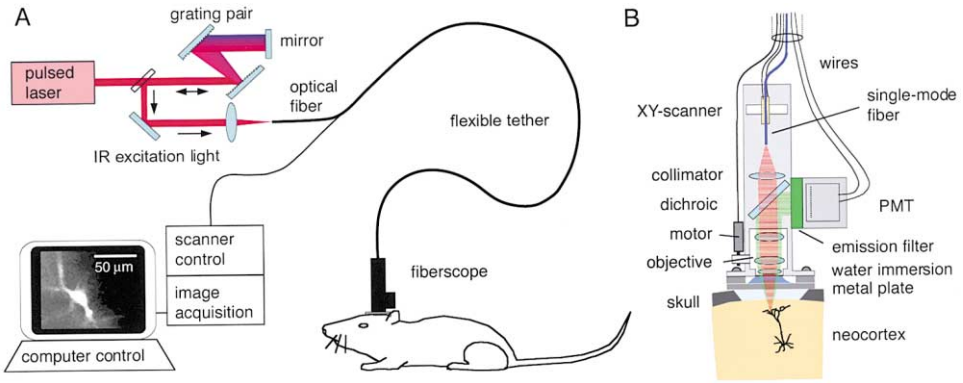

Figure 1. Two-Photon Fiberscope Setup

(A) Infrared pulsed laser light from a Ti:Sapphire laser is coupled into a single-mode optical fiber after double passing a pair of diffraction gratings for dispersion compensation. A flexible tether connects the laser components with a small microscope, which can be mounted on the head of a rat. Besides the optical fiber, the tether contains electrical wires, which are necessary to drive scanning, control focusing, and to provide supply voltage for the PMT and carry the PMT output signal.

(B) Microscope design. Light emerging from the fiber tip is collimated and focused through a water-immersion objective, which can be positioned with the help of a small motor. Lateral deflections of the fiber tip are used for scanning (see Figure 2). Fluorescence is detected with a small PMT. The miniature scanner and PMT, on the one hand, and the objective holder, on the other hand, are built as two separable units. The entire assembly can be mounted on a metal plate attached to the skull of a rat above a cranial window.

use for in vivo imaging in the neocortex. We show that stable imaging is possible in the cortex of awake, freely moving animals.

Results

Our goal was to develop a miniaturized two-photon excitation fluorescence microscope that is small and light enough to be carried by an adult rat. To this end, we designed a head-mountable microscope, which is connected to the bulky excitation laser and the optical setup via a flexible tether (Figure 1A). The key element of this tether is a single-mode optical fiber through which laser pulses for two-photon excitation are delivered. The microscope contains a miniature scanning device (described below), epifluorescence optics, and a small photomultiplier tube (PMT) (Figure 1B). The tether ($\sim$2 meters long) also contains a few electrical wires for microscope control and signal acquisition. Our current microscope is 7.5 cm long and weighs 25 g. This is comparable in size to chronic multielectrode implants (deCharms et al., 1999), which are routinely carried by adult rats. We have not yet attempted to reduce size and weight to their absolute engineering limits, and routes to further miniaturization and weight reduction will be explored in the Discussion.

Fiberscope Design

A detailed description of the mechanical and optical components is given in Experimental Procedures. Here, we address only the most fundamental issues, which had to be considered in the design of the microscope.

Two-Photon Excitation through Optical Fiber

Efficient two-photon excitation at moderate average powers generally is achieved using very brief (subpicosecond) laser pulses (Denk and Svoboda, 1997). Propagation of such so-called "ultrashort" pulses (for a collection of papers on ultrashort pulses see Gosnell and Taylor, 1991) through an optical fiber, however, results in significant temporal broadening of the pulses due to two different physical phenomena. The first of those is group-velocity dispersion (GVD) in the fiber, due to the fact that the speed of wave packets and therefore their arrival time after passage through the fiber varies with wavelength (Agrawal, 1995). Because frequency components from the long-wavelength ("red") part of the pulse spectrum travel faster in the fused silica material of the fiber than those from the short-wavelength ("blue") part, the pulse leaving the fiber is lengthened and "chirped" (frequency modulated). It is possible to compensate for GVD by giving the short-wavelength components a sufficient head start (negative "prechirp") so that blue and red components arrive at the fiber end at the same time. Prechirping can be accomplished with special arrangements of prisms (Fork et al., 1984) or diffraction gratings (Treacy, 1969). We used a grating pair whose distance was adjusted so that the amount of negative prechirp exactly compensated the positive chirp caused by the fiber (Figure 1A). This nearly restored the initial pulse width of about 100 fs at the fiber output for average powers $<$10 mW (pulse energies of $<$1 nJ).

At higher energies, pulse propagation is affected by a second effect, called "self-phase modulation" (SPM). SPM is caused by the dependence of the refractive index on the light intensity and is exacerbated in single-mode optical fibers due to the small beam diameter and the resulting large peak intensity (Agrawal, 1995). In contrast to GVD, which is a linear optical effect, SPM is a nonlinear effect and changes the wavelength spectrum. SPM leads to pulse lengthening and is difficult if not impossible to compensate for by prechirping. SPM-induced pulse broadening therefore currently limits the efficiency of two-photon excitation that can be achieved immediately at the end of optical fibers (if, unlike in our application, a recompression device can be inserted

after the end of the fiber, the transmission of higher pulse energies is possible). In our setup, SPM caused pulse lengthening to about 1 ps at the maximum average power used (~180 mW), even with optimal GVD compensation.

Objective Lens

Fluorescence excitation and collection depend strongly on the numerical aperture (NA). Most high NA objectives are, however, rather heavy. We therefore used a water-immersion objective (55×, NA 0.8, Syncotec) which was removed from its original holder and reassembled in a custom-made holder minimized in size and weight (objective weight now ~4 g). The working distance of this objective is sufficiently long (>1.5 mm) to permit imaging in the neocortex. Due to optical design constraints, the excitation beam did not completely fill the back aperture of the objective, meaning that the full NA was not used for excitation. This results in a slightly lower optical resolution but does not reduce the total fluorescence generated as long as the fluorescent objects contain the entire focal volume (Birge, 1986). A large NA is, nevertheless, crucial for efficient collection of the fluorescence light.

Fluorescence Detection

A major advantage of two-photon excitation is that it is confined to the focal spot (Denk and Svoboda, 1997). As a consequence, all emitted photons, scattered or not, are known to originate from the focal volume and can thus usefully contribute to the signal. In our microscope, we therefore realized a "whole-area" detection scheme (Denk et al., 1995) by placing the PMT as close as possible to the objective (Figure 1B).

Scanning

A compact scanning device was of critical importance in the microscope design. In the case of fiber illumination, a simple method to scan the focal spot is to move the tip of the fiber (Delaney and Harris, 1995). We achieved such scanning of the fiber tip using a piezoelectric bending element that induced flexural vibrations of the freestanding fiber end (Figure 2). Relatively large deflections of the tip could easily be induced when the piezoelectric element was excited near the mechanical resonance frequency of the fiber end (typically, 300–800 Hz). To allow two-dimensional scanning, the fiber end was stiffened in one direction so that vibrational resonance occurred at different frequencies in the two lateral directions (Figure 2A). Simultaneous excitation of vibrations at both frequencies then generated a two-dimensional scan pattern in the form of a Lissajous figure (Lissajous, 1855). The main features of this pattern (area coverage, resolution, and repeat frequency) are determined by the ratio of the two frequencies. Within the resonance widths, we selected the two frequencies so that a pattern densely covering the scanned area was produced (see Experimental Procedures). The motion of the fiber tip is completely determined by the voltage driving the piezoelectric element (which is a superposition of the *x* and *y* signal). However, the drive signals do not directly represent the position of the fiber tip because, particularly near resonance, a strong phase shift exists between driving force and response (Figure 2C). We could, nevertheless, reconstruct the tip position precisely from the *x* and *y* drive signals after correcting for that phase difference. Phase shifts were determined by directly measuring the scan pattern with a two-dimensional position-sensitive detector before an experiment. In addition, phases were fine tuned during the experiment by minimizing double and quadruple images, which result from errors in phase settings. The fluorescence intensities measured by the PMT were then assigned to the corresponding pixels in order to form an image (Figure 2D).

To enable measurements at high time resolution, we implemented a line scan mode by exciting the piezoelectric element with only one of the two resonance frequencies. This caused motion of the fiber tip along only one direction and in principle allows an increase of the time resolution up to one half of the oscillation period (~1–2 ms in our case). To get sufficient signal, we averaged fluorescence intensities over a few oscillation periods, resulting in a time resolution of 10 ms.

Vasculature Structure and Hemodynamics in the Neocortex

We first tested the suitability of the two-photon fiberscope for in vivo imaging in anesthetized, head-restrained rats. Blood plasma was stained by tail vein injection of fluorescently labeled dextrans (Kleinfeld et al., 1998), and cortical vasculature was imaged through a small craniotomy that was cut above somatosensory cortex. In 21 out of 23 rats injected, we obtained fiberscope images of cortical blood vessels near the surface and the capillary network underneath (Figure 3A). Individual capillaries could be studied in detail after zooming in (by reducing the amplitude of the voltage driving the fiber scanner). The maximum imaging depth was ~250 μm. This depth penetration is roughly half that obtained using a directly coupled two-photon microscope (Kleinfeld et al., 1998; Helmchen et al., 1999).

To measure blood-cell movement with high temporal resolution, we used the line scan mode (Figure 3B). As in previous studies employing standard laser-scanning microscopes (Dirnagl et al., 1992; Kleinfeld et al., 1998), individual blood cells appeared as moving shadows, since they exclude the dye. In the line scan images, this resulted in tilted dark bands, the slopes of which were used to measure the speed of blood cell flow. In 12 capillaries from four rats, the speed ranged from 0.25 to 1.38 mm/s (average 0.84 ± 0.47 mm/s; mean ± SD), similar to the values reported in a previous study in layers two through four of rat somatosensory cortex (Kleinfeld et al., 1998).

Dendritic Morphology and Calcium Transients

Next, we imaged individual neurons filled with the calcium indicator Calcium green-1 in layer 2/3 in vivo (Figure 4). Intracellular recordings were obtained from layer 2/3 neurons in 28 anesthetized rats. Of 32 indicator-injected neurons (recordings for >10 min), 21 neurons were found using the two-photon fiberscope. In 13 cases, dendritic processes were clearly resolved. Figure 4A shows examples of fluorescence images in which dendrites are visible. Dendrites could be seen down to 200–250 μm below the surface; in the best cases, dendritic spines were resolved on individual branches at high magnification (Figure 4Ad).

The line scan mode permitted measurements of den-

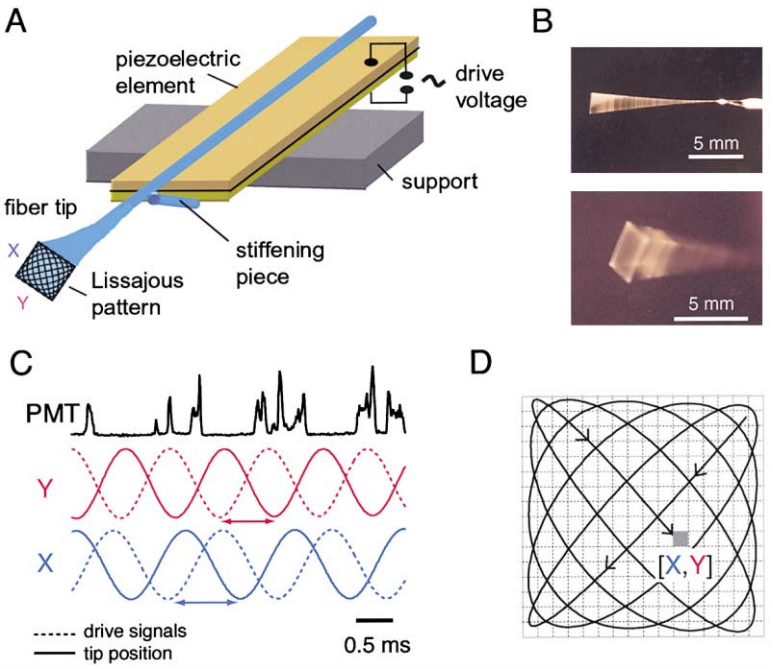

Figure 2. Fiber Scanning and Image Reconstruction

(A) Resonant fiber vibration as an area-scanning mechanism. The optical fiber end with the fiber jacket stripped off is glued to a piezoelectric bending element leaving a short end (protruding 1–2 cm) free to vibrate. Lateral deflections of the tip by more than 1 mm can be induced by driving the piezoelectric element at the fiber end's vibrational resonance frequency. Two-dimensional (area) scanning is achieved by stiffening the tip in one direction with a short stiffening rod and driving the bending element with a superposition of the two resulting resonance frequencies. (B) Photographs of a vibrating fiber tip in side view (top) and—with simultaneous excitation at both resonance frequencies—in front view (bottom). Several seconds exposure time. (C) Image reconstruction. The *x* and *y* drive signals (shown before their superposition) are used as position reference signals after correcting for the phase shifts between driving forces and fiber tip position (indicated by arrows). Reference signals and the PMT output signal are sampled at 100 kHz/channel, and an image is formed by assigning the PMT intensity values to the corresponding pixel. Pixel assignment is exemplified in (D) for a 16 × 16 pixel image array. Only part of the trajectory forming the Lissajous scan pattern is shown in (D).

dritic calcium dynamics in vivo (Figure 4B). In five cells, transient changes in Calcium green-1 fluorescence (ΔF/F in the range of 40%–200%) were evoked in the proximal apical dendrite by action potentials that had been triggered by current injections through the intracellular electrode. The observed calcium transients were similar to those reported in previous in vivo studies (Svoboda et al., 1997, 1999), although with a slightly slower time course (700–900 ms decay time), presumably caused by the relatively high indicator concentration used in the electrodes (up to 10 mM).

In summary, these measurements in anesthetized, head-stabilized rats demonstrate that the fiberscope is suitable for in vivo imaging in a manner similar to a fixed two-photon microscope, although currently with somewhat reduced depth penetration and resolution. However, the fiberscope was not designed to replace mirror-scanned instruments in stationary applications but, instead, to enable imaging in moving animals.

Imaging in Freely Moving Animals

In the next set of experiments (n = 7), the fiberscope was mounted on the head of the rat following staining of the blood plasma during anesthesia (isoflurane). Then, the animal was placed in a cage and allowed to recover from anesthesia. The cage was placed on a freely turning

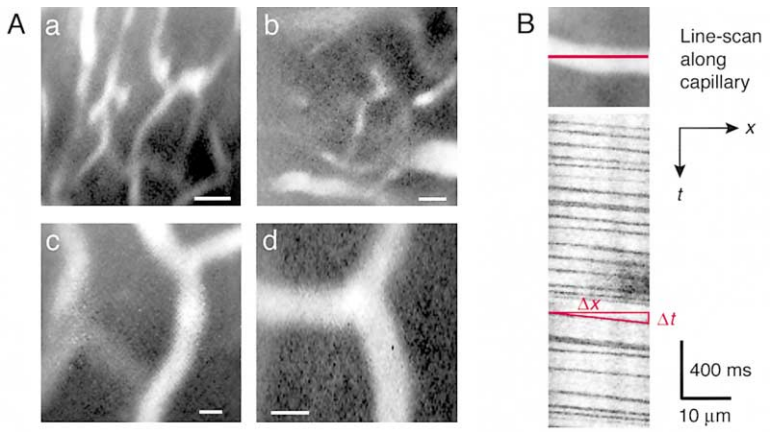

Figure 3. In Vivo Imaging of Cortical Vasculature and Capillary Blood Flow

(A) Two-photon fiberscope images of fluorescently labeled vasculature in somatosensory cortex of rat (anesthetized, head restrained). Large vessels and the capillary network are visible in (Aa) and (Ab). Individual capillaries are shown at higher magnification in (Ac) and (Ad). Images are from four different rats and were acquired with 4–5 s exposure time. Scale bars are 20 μm (Aa and Ab) and 5 μm (Ac and Ad). Imaging depths were 50 μm (Aa), 200 μm (Ab), and 100 μm (Ac and Ad).

(B) Blood cell flow measured in an individual capillary using a line scan along the capillary axis (top). Line scans were generated by exciting vibration of the fiber tip in only one direction. Flowing blood cells appear as dark bands in the line scan image (bottom). Blood cell speed is calculated from the slope of the bands as $v = \Delta x/\Delta t$ (0.25 mm/s for the capillary shown). Effective time resolution is 10 ms.

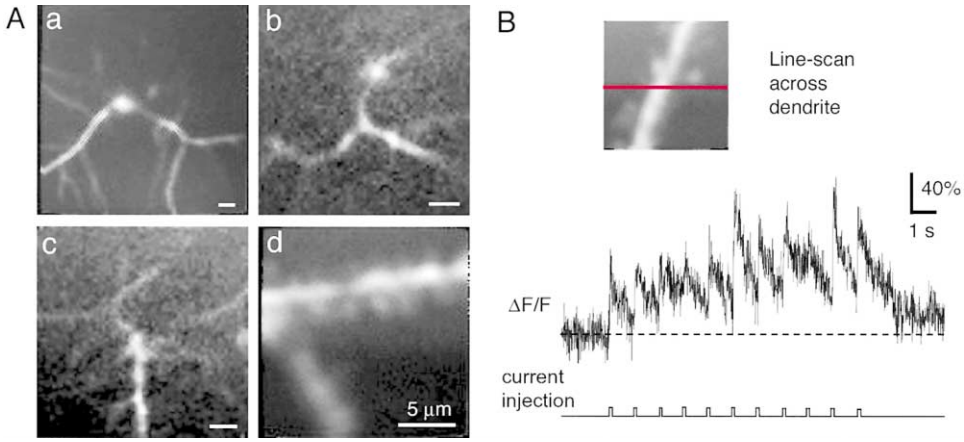

Figure 4. In Vivo Imaging of Layer 2/3 Neurons and Dendritic Calcium Dynamics

(A) Fiberscope images of layer 2/3 neurons and dendrites in somatosensory cortex of rats (anesthetized, head restrained). Neurons were filled with Calcium green-1 via intracellular recording electrodes. Image examples of dendrites from three different cells are shown in (Aa)–(Ac). Enlargement of a dendritic branch in (Aa) revealed dendritic spines (Ad). Scale bars are 10 μm in (Aa)–(Ac). Imaging depths were 130 μm (Aa), 120 μm (Ab), 160 μm (Ac), and 120 μm (Ad).

(B) Calcium green-1 fluorescence transients in a proximal dendrite of a layer 2/3 neuron. Fast transients were measured using a line scan across the dendrite (top). Current injections at 1 s intervals elicited bursts of one to four action potentials, which evoked calcium transients decaying with a time constant of ~750 ms. Time resolution was 10 ms.

table to prevent extensive twisting of the fiberscope tether. After recovery from anesthesia, time series of cortical vasculature images were recorded in the awake, unrestrained animals during various states of animal motion. Animal behavior was documented simultaneously with a video camera. The image was stable during periods of little or no head motion, for example, while the animal was resting but chewing (Figure 5). There was no apparent difference compared to image series acquired during anesthesia with the head immobilized. Imaging was relatively stable during moderate movements of the animal's head, such as those that occurred during turning of the body and steady walking, although images sometimes shifted laterally (Figure 5), and changes in the focal plane position could occur. The lateral shifts were on the order of a few tens of micrometers and possibly were due to movements of the brain relative to the skull or to slight shifts or tilts of the microscope relative to the skull. Image stability was not maintained, however, during rapid movements of the head or sudden contact with the wall of the cage. In these cases, movements occurred on a time scale faster than the frame acquisition; images therefore were distorted, and sometimes the Lissajous scan pattern became partially visible. Following these brief periods of disturbance, images usually stabilized again although permanent shifts in the imaging position sometimes occurred (Figure 5). In summary, these measurements demonstrate that it is possible to acquire fluorescence images with high spatial resolution in the brain of freely moving animals.

Unfortunately, we have not quite succeeded in demonstrating what clearly is the ultimate goal of our efforts: functional imaging of neurons in freely moving animals. We still believe that the technology described in this paper will eventually allow us to reach this goal. Several factors are acting as handicaps. First, as in previous in vivo imaging studies (Svoboda et al., 1997; Helmchen et al., 1999), we were forced to label cells individually via micropipettes. The location of the cell cannot be precisely controlled due to the somewhat stochastic process of establishing a stable recording. Imaging conditions therefore are not always optimal (overlying blood vessels for example act as cylindrical lenses and destroy the focus). As a result, it is sometimes not possible to find cells even with the fixed microscope. Second, different from those earlier studies, we need to retract the electrode after filling the cell, which frequently results in the destruction of the cell. In addition, after mounting the fiberscope on the head of the rat, no electrode is available as guide to the neuron. This reduces the probability of finding the labeled cell, as in the case of imaging pyramidal neurons with deep somata (Helmchen et al., 1999). The difficulties of finding individually labeled cells are exacerbated by the limited lateral mobility and reduced imaging depth of the head-mounted fiberscope. One way to overcome these problems would be labeling of cell populations with genetically encoded functional probes, which may be possible in the near future. Both the lateral mobility and the depth penetration of the fiberscope might be improved in the future by a number of conceivable yet nontrivial technical refinements (see Discussion).

Discussion

We have built a miniaturized two-photon microscope and demonstrated that it is suitable for fluorescence imaging in freely moving animals. The spatiotemporal resolution of the fiberscope is sufficient to resolve dendritic morphology and calcium transients in cortical layer 2/3. Movement artifacts were found to be tolerable during periods of moderate motion of the animal's head. The novel microscope holds the promise of measuring

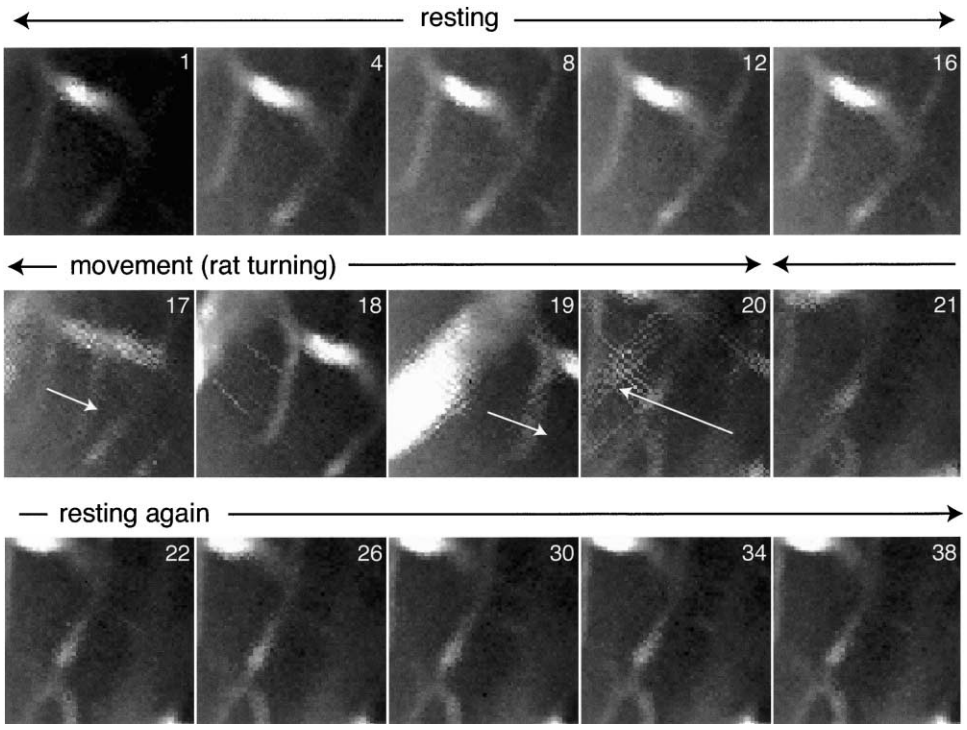

Figure 5. Imaging in Awake, Freely Moving Rats

Sample frames from an image series of fluorescently labeled blood in capillaries acquired with the two-photon fiberscope in an awake rat (0.5 s frame duration; numbers indicate frame number). The image was stable while the rat was resting (frames 1 through 16; every fourth frame shown). During frames 17 to 20, the rat moved and turned its body around. This motion caused shifts of the image as indicated by the arrows. In frame 20, part of the Lissajous scan pattern can be seen, because shifting occurred during the frame acquisition. Following the movement, the image stabilized again, although at a slightly different position (frames 22 through 38). Based on the diameter of capillaries (about 5–6 μm), we estimate the field of view to be ~65 μm on side.

subcellular activity and hence studying dendritic integration in animals free to move about.

Microscope Miniaturization Using Fiber Optics

In our design, a single-mode fiber is used for both delivery of laser pulses for two-photon excitation and scanning of the illumination spot. In several respects, our fiberscope differs from previously developed miniaturized fluorescence microscopes using fiber optics (Delaney and Harris, 1995). Those fiberscopes employ single-photon excitation and are based on the idea that confocality emerges naturally if a single-mode fiber is used for illumination and fluorescence collection because the fiber core acts as confocal pinhole. Miniature confocal microscopes have been applied in vivo, for example, to image microvasculature and nerve fibers in rat colon (Papworth et al., 1998) and mouse skin (Bussau et al., 1998) and cell nuclei in mouse peritoneum (Sabharwal et al., 1999). No application to imaging in the CNS has been reported so far. This might well be due to the limited depth penetration that plagues confocal microscopy in scattering tissue (Denk and Svoboda, 1997).

By combining two-photon excitation through the optical fiber with whole-area detection, we can exploit the advantages that two-photon excitation offers in a miniaturized setting. The first of those advantages is that excitation light scattering is reduced because of the longer wavelength, thus improving depth penetration. The second advantage is that excitation is confined to the focal volume, which reduces out-of-focus photodamage and, even more important, permits much more efficient fluorescence collection than in a confocal microscope (Denk and Svoboda, 1997). A problem peculiar to two-photon excitation through a fiber is the intensity-dependent pulse broadening caused by fiber nonlinearities (Agrawal, 1995). In our case, pulses were broadened to ~1 ps at ~180 mW average output power. As two-photon absorption depends inversely on the pulse length, this means that the excitation efficiency is reduced at high intensities. Nevertheless, we were able to image capillaries and dendrites down to 250 μm below the brain surface. In order to improve the signal-to-noise and to increase the depth penetration to what can be achieved with a directly coupled two-photon microscope (~500–600 μm), it will be crucial to further optimize two-photon excitation through optical fibers. The use of special large-core fibers and employment of more sophisticated pulse compression schemes may in the future allow us to reduce the effect of fiber nonlinearities and to obtain pulses in the 100 fs range at the fiber output even at or above 200 mW average power. Alternatively, excitation might be improved by using picosecond pulses from the start, as they can propagate through the fiber at high power with negligible dispersive and nonlinear broadening (the large average power delivered to the tissue would still be a concern).

The use of resonant flexural vibrations of the fiber tip as scanning mechanism results in a compact and lightweight scanner. Compared to other miniature scan devices, e.g., micromachined mirrors (Dickensheets and Kino, 1996; Hofmann et al., 1999), the fiber scanner is simple and based on the application of a single, readily available piezoelectric bending element. Lissajous scanning relies on frequency splitting the fiber resonance, which requires an anisotropy of the fiber bending stiffness. This can be achieved, for example, with the help of a diagonal strut (Figure 2). A single bending element is sufficient to induce two-dimensional vibration, as long as deflections of the bending element are coupled to both vibrational modes. Our fiberscope produces stable and reproducible images in freely moving rats during rest and moderate motion. Sudden movements, however, lead to image shifts that probably are dominated by motion of the brain or skull relative to the microscope rather than by distortions of the fiber tip motion. Shifts of the skull relative to the microscope might be reduced in the future, using a more stable mounting method, but shifts due to movement of the brain relative to the skull are, of course, independent of the microscope design.

Technological Outlook

Further technical refinements are desirable to improve the performance of the fiberscope as a practical tool for imaging neuronal activity in behaving animals. One example is a mechanical design that not only allows remote focusing but also remote positioning of the field of view. This could be achieved, for example, with the help of small motors and would alleviate the difficulty of finding individual dye-filled neurons. A remote fine-positioning ability would also permit easy readjustment of the field of view following lasting lateral shifts that occasionally occur during animal movements (see Figure 5). In addition, images of the surface blood vessel pattern might be produced using the backscattered light, providing position landmarks for finding a previously filled neuron. Another possibility to overcome the problems of working with individual neurons is to label populations of neurons using other staining techniques, in particular, by applying genetically encoded indicators based on green fluorescent protein (GFP). Recently, two-photon microscopy has been used to study dynamic changes of dendritic morphology in vivo following sparse labeling of rat cortical neurons with GFP using viral transfection (Lendvai et al., 2000). Similarly, cortical neurons may be labeled with GFP-based indicators that are sensitive to calcium (Baird et al., 1999; Miyawaki et al., 1997; Nakai et al., 2001) or chloride (Kuner and Augustine, 2000). This approach would simplify the application of the fiberscope by allowing the selection of a labeled neuron at a location suitable for imaging. In addition, labeling of neuronal populations may permit visualization of the activity pattern in cell groups following sensory stimulation and—using the fiberscope—during different behavioral states. Another possibility is the measurement of presynaptic calcium dynamics in specific cortical projection pathways that have been labeled by injection and transport of dextran-conjugated calcium indicators (Kreitzer et al., 2000).

Further miniaturization of the microscope might involve the development of a custom objective lens. In addition, fluorescence can be collected through a large-core (multimode) fiber and detected by a fixed PMT. Detection at the fixed end of the tether would not only reduce the weight of the fiberscope but also abolish the restrictions on detector type, size, and weight and enable simultaneous imaging in multiple wavelength channels. With custom optics, it might be possible to develop a "slim" version of the front end of the fiberscope with an outer diameter small enough to allow insertion into the brain. Though requiring removal of some brain tissue, such an "endoscopic" approach may allow two-dimensional imaging and calcium measurements in deeper brain structures, such as the hippocampus, extending the concept of deep fluorescence measurements using fiber optic probes (Davis and Schmidt, 2000). In summary, these various technological refinements are likely to make the fiberscope more efficient, more compact, and easier to use. In principle, a reduction in weight to less than 5 g appears feasible, which then would permit application to mice.

Applications

A major motivation for the development of the fiberscope was to enable studies of neural activity in behaving animals. Although we have not yet succeeded in imaging single-cell activity in a freely moving rat, we have overcome most of the crucial technical hurdles in the way of such experiments. We have demonstrated both that dendritic activity can be measured in vivo using the fiberscope and that the imaging stability even in moving animals is sufficient for measurements on a cellular scale. Fiberscope measurements thus should allow studies of the modulation of dendritic excitability during sleep and wakefulness and on how changes in excitability might define certain behavioral states. Although fiberscope images were blurred during sudden movements, images stabilized again quickly, so that not much of the record is lost. We therefore expect that it will be possible to image neural activity during periods of a behavioral task that involve only little motion. It should, for example, be possible to follow dendritic activity during the decision-making period that preceeds explicit behavior.

Experimental Procedures

Animals and Surgery

Adult Sprague-Dawley rats (150–500 g) were used for experiments. All procedures were approved by the Institutional Animal Care and Use Committee. For surgical preparation, rats were anesthetized either with urethane (1.5 g/kg body weight), ketamine (75 mg/kg ketamine, 3.8 mg/kg xylazine, 0.75 mg/ml acepromazine), or isoflurane (1%–1.5%). In experiments involving imaging in freely moving animals, isoflurane anesthesia was used during surgery. Animal temperature was monitored throughout anesthesia with a rectal probe and maintained at 36°C–37°C using a heating blanket (Harvard Instruments).

Surgical procedures were similar to those described previously (Svoboda et al., 1999). The skull of the rat was exposed and cleaned, and a metal plate was attached to the skull with dental acrylic cement. Two screws secured to the skull provided additional stabilization. The center hole of the base plate was positioned above somatosensory cortex in an area corresponding to the hindlimb/hindpaw region. A small craniotomy (2–3 mm diameter) was opened

above this area, and the dura was carefully removed. To dampen heartbeat- and breathing-induced brain motion, the craniotomy was filled with agarose (1.5%, Type III-A, Sigma) in artificial cerebral spinal fluid (ACSF; 125 mM NaCl, 5 mM KCl, 10 mM glucose, 10 mM HEPES, 2 mM $CaCl_2$, and 2 mM $MgSO_4$, pH 7.3–7.4 with NaOH) and covered with a coverslip. For blood vessel imaging, this cranial window was fully sealed with dental acrylic cement. In experiments involving intracellular recordings, the coverslip was left unsealed on one side so that electrodes could be inserted at a shallow angle through the agar.

Labeling

All labeling procedures were performed during anesthesia and during head fixation. Blood plasma was stained by tail vein injection of a 0.3–0.5 ml bolus of FITC- or rhodamine-labeled dextran (77 kDa, 5% w/v in ACSF; both from Sigma) (Kleinfeld et al., 1998). This resulted in bright and temporally stable labeling of the cortical vasculature.

Individual neurons in layer 2/3 were filled with the calcium indicator dye Calcium green-1 (Molecular Probes) by iontophoresis from the intracellular recording electrodes. Electrodes (borosilicate glass, 50–100 MΩ) were inserted at a shallow angle through the agar from the medial-lateral side. The electrode solution contained 0.4 M KAcetate and 3–10 mM Calcium green-1 (pH 7.3, buffered with HEPES). Recordings were made with a high impedance amplifier (Neurodata, Cygnus Technology, PA).

Mechanical and Optical Design

The fiberscope setup comprised two components: the laser system and the head-mounted microscope, which were connected via fiber optics (Figure 1). A Ti:Sapphire laser (Tsunami; Spectra Physics), pumped by a 10 W diode-pumped solid-state laser (Millenia X; Spectra Physics), provided ultrashort laser pulses (initial pulse width ~100 fs) at a wavelength of 820–850 nm. Laser light was coupled into the single-mode fiber (FS-4224, 5.5 μm mode field diameter; 3M) using an aspheric lens (f = 18.4 mm; NA 0.15; Geltech). To compensate for fiber dispersion, laser pulses were negatively prechirped before coupling to the fiber using a pair of diffraction gratings (400 grooves/mm; 9.7° blaze angle; Richardson Gratings Lab) in double-pass configuration (Treacy, 1969). For a 1.7 meters long piece of the single-mode fiber, a prechirp of ~−74,000 fs^2 nearly restored the initial pulse width at low average output power (<10 mW). At higher power, self-phase modulation (Agrawal, 1995) caused pulse broadening to about 1 ps at 180 mW.

The microscope consisted of a titanium tube (1.3 cm diameter), which contained the miniature scan device and epifluorescence optics. The bare fiber was glued on a small piezoelectric bending element (~2 mm × 8 mm, 0.5 mm thick; EDO) to induce resonant vibrations of a 1–2 cm long freestanding fiber end. The stiffening rod (e.g., a short piece of bare fiber) was glued to the fiber (at a distance of ~3 mm from the edge of the bending element) and to the lower sheet of the element. In front view, the stiffening rod formed an angle of ~45° with the surface of the bending element so that vibrations in the two diagonal directions absorbed about equal power. Driving the bending element with a superposition of the two resonance frequencies resulted in an area scan in the form of a Lissajous figure (see below). The beam emerging from the fiber tip was collimated with an aspheric lens (f = 11 mm; NA 0.25; Geltech) and focused through a water-immersion objective (55×, NA 0.8; Syncotec, Technical Instruments). The objective could slide inside its holder (coated with vacuum grease) and was positioned using a small DC motor (3 mm "smoovy" gearmotor SPH39003, gear ratio 1:125; RMB Miniature Bearings, NJ) attached to the outside of the holder. A threaded rod connected to the motor axle moved a shuttle nut that was rigidly connected to the objective. Fluorescence light was collected through the objective, deflected by a dichroic mirror (Cold mirror; Edmund Scientific) and detected with a small PMT (RU5600; Hamamatsu). A 5 mm thick colored-glass filter (BG39, Schott) in front of the PMT was used to block the exitation light. For alignment purposes, the microscope was built as two separable components. This arrangement permitted us to use the objective as a regular microscope objective in combination with eyepieces before mounting the scanning and detection module. In experiments on anesthetized rats, the fiberscope was attached to a focusing unit (Nikon) fixed to an xy translation table to allow three-dimensional movement.

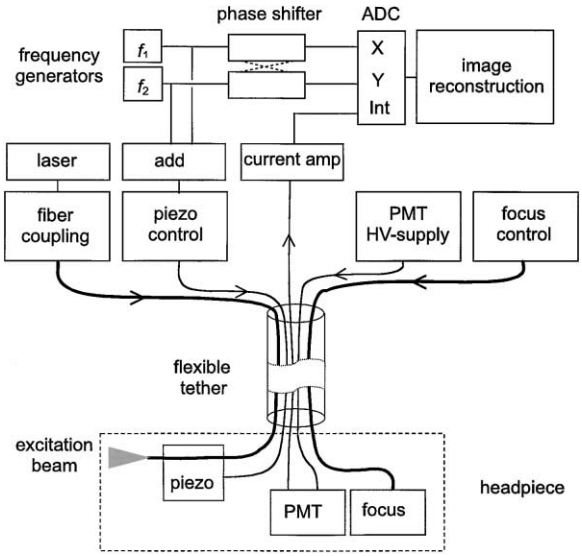

Figure 6. Flowchart of the Fiberscope Setup

Two frequency generators produce sinusoidal voltages at the two resonance frequencies of the fiber tip. The superposition of these voltages is used to drive the piezoelectric bending element. The PMT current signal is amplified and digitized for image reconstruction together with the phase-shifted versions of the x and y drive signals. The flexible tether also contains the high-voltage power supply for the PMT and the wires for controlling the focusing motor.

Lissajous Scanning

Efficient use of the fiber scanner relies on an appropriate choice of frequencies. It was therefore important to characterize the vibrational resonances each time a new fiber end was installed. For 1–2 cm long fiber tips, frequencies were in the range of 1000–250 Hz (the resonance frequency depends inversely on the square of the tip length). Near resonance deflections of more than 1 mm were easily achieved (Figure 2B). Half-widths of the resonance curves (Δf) were ~10 Hz (Q = f/Δf about 40). Within this width, we chose the two frequencies (f_x and f_y) for driving the fiber scanner with the goal of obtaining a self-repeating scan pattern with high area coverage. Though not absolutely necessary, this choice of a stable pattern repeating itself with a certain frequency is convenient for image reconstruction purposes. The main determinant of the scan pattern is the ratio of the frequencies. A repetitive pattern is obtained if this ratio is a rational number, i.e., if $f_x/n_x = f_y/n_y = f_R$, where n_x, n_y are the smallest possible integers with the ratio n_x/n_y equal to f_x/f_y, and f_R is the pattern repeat frequency. The numbers n_x and n_y roughly determine the resolution of the pattern (the density of the intersections of the trajectory). Based on these considerations, our strategy for the choice of frequencies was as follows. First, frequencies were selected as close as possible to the peak of the resonances to ensure that the lateral vibration modes were nearly orthogonal. Second, the frequency ratio was adjusted so that a repeat frequency of 2 Hz resulted, because this frequency provides sufficient spatial resolution and enables online image reconstruction and display. For frequencies in the range of 300–800 Hz, n_x and n_y therefore were in the range of 150–400. This ensured that all pixels were sampled at least once during a 0.5 s frame with a pixel resolution of either 64 × 64 or 128 × 128 used for image reconstruction.

Fiberscope Control and Image Acquisition

Figure 6 shows a flowchart of the fiberscope components and illustrates the composition of the flexible tether. Two digital frequency generators (model DS345; Stanford Research Systems) with syn-

chronized time bases provided sinusoidal voltages at the chosen frequencies. The electronic superposition of these signals was the input to a high-voltage amplifier (0–100V, PZ-150; Burleigh) driving the piezoelectric bending element. The output signals of the frequency generators were at the same time fed through custom-built electronics that mimicked the mechanical response of the fiber. This circuit permitted us to independently shift the *x* and *y* signal in their phase and, in addition, to eliminate some residual cross-talk between the *x* and *y* direction ($<5\%$ of amplitude). The output signals of this circuit were then used as accurate reference signals for the actual position of the fiber tip. Amplitude and phase settings were adjusted by comparing the generated reference signals with the actual scan pattern, which was directly measured with a position-sensitive detector (ON-TRAK Photonics, CA). In addition, even small errors in phase setting became apparent during the experiment as doubling of edge structures in the reconstructed images and could be corrected for empirically.

For image reconstruction, the PMT current signal was preamplified (Series 1211 Ithaco, Ithaca, NY) and digitized together with the *x* and *y* reference signals at 100 kHz/channel (MIO-16E-1 board; National Instruments). The PMT intensity values were assigned to the pixel corresponding to the *x* and *y* readout (the total number of pixels was chosen beforehand; typically, we used 64×64 or 128×128 arrays). This assignment was performed online using custom-written software in LabView (National Instruments). In a Lissajous scan pattern, individual pixels are not sampled with the same frequency (pixels near the image edges are "hit" more often). To adjust for this uneven scan density and in order not to waste information, a second array was held in the background in which the number of hits was stored for each pixel. The final image for one exposure time then contained the average intensity value for each pixel. The same strategy was applied in line scan mode.

Acknowledgments

We thank G. Buzsaki for discussions; and M. Brecht and D.J. Waters for critically reading the manuscript. This work was supported by Lucent Technologies and the Whitehall Foundation. F.H. acknowledges support by a postdoctoral fellowship from the Human Frontier Science Program.

Received April 30, 2001; revised July 19, 2001.

References

Agrawal, G.P. (1995). Nonlinear Fiber Optics, Second Edition (San Diego: Academic Press).

Baird, G.S., Zacharias, D.A., and Tsien, R.Y. (1999). Circular permutation and receptor insertion within green fluorescent proteins. Proc. Natl. Acad. Sci. USA *96*, 11241–11246.

Birge, R.R. (1986). 2-photon spectroscopy of protein-bound chromophores. Acc. Chem. Res. *19*, 138–146.

Borst, A., and Egelhaaf, M. (1992). In vivo imaging of calcium accumulation in fly interneurons as elicited by visual motion stimulation. Proc. Natl. Acad. Sci. USA *89*, 4139–4143.

Bussau, L.J., Vo, L.T., Delaney, P.M., Papworth, G.D., Barkla, D.H., and King, R.G. (1998). Fibre optic confocal imaging (FOCI) of keratinocytes, blood vessels and nerves in hairless mouse skin in vivo. J. Anat. *192*, 187–194.

Buzsaki, G., and Kandel, A. (1998). Somadendritic backpropagation of action potentials in cortical pyramidal cells of the awake rat. J. Neurophysiol. *79*, 1587–1591.

Davis, M.D., and Schmidt, J.J. (2000). In vivo spectrometric calcium flux recordings of intrinsic caudate-putamen cells and transplanted IMR-32 neuroblastoma cells using miniature fiber optrodes in anesthetized and awake rats and monkeys. J. Neurosci. Meth. *99*, 9–23.

deCharms, R.C., Blake, D.T., and Merzenich, M.M. (1999). A multielectrode implant device for the cerebral cortex. J. Neurosci. Meth. *93*, 27–35.

Delaney, P.M., and Harris, M.R. (1995). Fiberoptics in confocal microscopy. In The Handbook of Biological Confocal Microscopy, J.B. Pawley, ed. (New York: Plenum Press), pp. 515–523.

Denk, W., and Svoboda, K. (1997). Photon upmanship: why multiphoton imaging is more than a gimmick. Neuron *18*, 351–357.

Denk, W., Piston, D.W., and Webb, W.W. (1995). Two-photon molecular excitation in laser-scanning microscopy. In The Handbook of Biological Confocal Microscopy, J.B. Pawley, ed. (New York: Plenum Press), pp. 445–458.

Denk, W., Yuste, R., Svoboda, K., and Tank, D.W. (1996). Imaging calcium dynamics in dendritic spines. Curr. Opin. Neurobiol. *6*, 372–378.

Dickensheets, D.L., and Kino, G.S. (1996). Micromachined scanning confocal optical microscope. Optics Lett. *21*, 764–766.

Dirnagl, U., Villringer, A., and Einhaupl, K.M. (1992). In-vivo confocal scanning laser microscopy of the cerebral microcirculation. J. Microsc. *165*, 147–157.

Eilers, J., and Konnerth, A. (1997). Dendritic signal integration. Curr. Opin. Neurobiol. *7*, 385–390.

Fee, M.S. (2000). Active stabilization of electrodes for intracellular recording in awake behaving animals. Neuron *27*, 461–468.

Fork, R.L., Martinez, O.E., and Gordon, J.P. (1984). Negative dispersion using pairs of prisms. Optics Lett. *9*, 150–152.

Gosnell, T.R., and Taylor, A.J. (1991). Selected Papers on Ultrafast Laser Technology (Bellingham: SPIE Optical Engineering Press).

Häusser, M., Spruston, N., and Stuart, G.J. (2000). Diversity and dynamics of dendritic signaling. Science *290*, 739–744.

Helmchen, F., Svoboda, K., Denk, W., and Tank, D.W. (1999). In vivo dendritic calcium dynamics in deep-layer cortical pyramidal neurons. Nat. Neurosci. *2*, 989–996.

Hofmann, U., Mühlmann, S., Witt, M., Dörschel, K., Schütz, R., and Wagner, B. (1999). Electrostatically driven micromirrors for a miniaturized confocal laser scanning microscope. SPIE *3878*, 29–38.

Kleinfeld, D., Mitra, P.P., Helmchen, F., and Denk, W. (1998). Fluctuations and stimulus-induced changes in blood flow observed in individual capillaries in layers 2 through 4 of rat neocortex. Proc. Natl. Acad. Sci. USA *95*, 15741–15746.

Kreitzer, A.C., Gee, K.R., Archer, E.A., and Regehr, W.G. (2000). Monitoring presynaptic calcium dynamics in projection fibers by in vivo loading of a novel calcium indicator. Neuron *27*, 25–32.

Kuner, T., and Augustine, G.J. (2000). A genetically encoded ratiometric indicator for chloride: Capturing chloride transients in cultured hippocampal neurons. Neuron *27*, 447–459.

Lendvai, B., Stern, E.A., Chen, B., and Svoboda, K. (2000). Experience-dependent plasticity of dendritic spines in the developing rat barrel cortex in vivo. Nature *404*, 876–881.

Lissajous, J.A. (1855). Note sur une méthode nouvelle applicable à l'étude des mouvements vibratoires [On a novel method applicable to the study of vibrations]. Comptes Rendus des Séances de l'Academie des Sciences *41*, 814–817.

Miyawaki, A., Llopis, J., Heim, R., McCaffery, J.M., Adams, J.A., Ikura, M., and Tsien, R.Y. (1997). Fluorescent indicators for Ca^{2+} based on green fluorescent proteins and calmodulin. Nature *388*, 882–887.

Nakai, J., Ohkura, M., and Imoto, K. (2001). A high signal-to-noise Ca^{2+} probe composed of a single green fluorescent protein. Nat. Biotech. *19*, 137–141.

O'Malley, D.M., Kao, Y.-H., and Fetcho, J.R. (1996). Imaging the functional organization of zebrafish hindbrain segments during escape behaviors. Neuron *17*, 1145–1155.

Papworth, G.D., Delaney, P.M., Bussau, L.J., Vo, L.T., and King, R.G. (1998). In vivo fiber optic confocal imaging of microvasculature and nerves in the rat vas deferens and colon. J. Anat. *192*, 489–495.

Pare, D., Lang, E.J., and Destexhe, A. (1998). Inhibitory control of somatodendritic interactions underlying action potentials in neocortical pyramidal neurons in vivo: an intracellular and computational study. Neuroscience *84*, 377–402.

Rector, D.M., Poe, G.R., and Harper, R.M. (1993). Imaging of hippo-

campal and neocortical neural activity following intravenous cocaine administration in freely behaving cats. Neuroscience *54*, 633–641.

Rector, D.M., Poe, G.R., Redgrave, P., and Harper, R.M. (1997). A miniature CCD video camera for high-sensitivity light measurements in freely behaving animals. J. Neurosci. Meth. *78*, 85–91.

Regehr, W.G., and Tank, D.W. (1994). Dendritic calcium dynamics. Curr. Opin. Neurobiol. *4*, 373–382.

Sabharwal, Y.S., Rouse, A.R., Donaldson, L., Hopkins, M.F., and Gmitro, A.F. (1999). Slit-scanning confocal microendoscope for high-resolution in vivo imaging. Appl. Optics *38*, 7133–7144.

Single, S., and Borst, A. (1998). Dendritic integration and its role in computing image velocity. Science *281*, 1848–1850.

Sobel, E.C., and Tank, D.W. (1994). In vivo Ca^{2+} dynamics in a cricket auditory neuron: An example of chemical computation. Science *263*, 823–826.

Svoboda, K., Denk, W., Kleinfeld, D., and Tank, D.W. (1997). In vivo dendritic calcium dynamics in neocortical pyramidal neurons. Nature *385*, 161–165.

Svoboda, K., Helmchen, F., Denk, W., and Tank, D.W. (1999). Spread of dendritic excitation in layer 2/3 pyramidal neurons in rat barrel cortex *in vivo*. Nat. Neurosci. *2*, 65–73.

Treacy, E.B. (1969). Optical pulse compression with diffraction gratings. IEEE J. Quant. Elec. *5*, 454–458.

Yuste, R., and Tank, D.W. (1996). Dendritic integration in mammalian neurons: a century after Cajal. Neuron *16*, 701–716.

Yuste, R., Lanni, F., and Konnerth, A. (1999). Imaging Neurons: A Laboratory Manual (Cold Spring Harbor, NY: Cold Spring Harbor Laboratory Press).